Polymer Journal (2018) 50:337–345
https://doi.org/10.1038/s41428-017-0021-7

ORIGINAL ARTICLE

Self-association behavior of amphiphilic molecules based on incompletely condensed cage silsesquioxanes and poly(ethylene glycol)s

Hiroaki Imoto[1] · Ryoichi Katoh[1] · Tomoko Honda[2] · Shin-ichi Yusa[2] · Kensuke Naka[1]

Received: 12 October 2017 / Revised: 3 December 2017 / Accepted: 6 December 2017 / Published online: 6 February 2018

Abstract

Polyhedral oligomeric silsesquioxane (POSS) is an important building block for constructing organic-inorganic hybrid molecules or polymers. In this work, we report amphiphilic, incompletely condensed POSSs (IC-POSSs) possessing various substituents on the seven silicon atoms and two kinds of poly(ethylene glycol)s (PEGs) with different chain lengths. The IC-POSS cores possessed comparable thermal stability to that of the completely condensed POSS (CC-POSS) analogs, despite their open cage structure. The amphiphilic IC-POSSs formed micelles of different sizes and had polydispersity indices (PDIs) that were dependent on the substituents and the PEG chain length. Additionally, the lower critical solution temperatures (LCSTs) were observed for amphiphilic IC-POSSs possessing shorter PEG chains, while aqueous solutions of those with longer PEG chains showed high transmittance even at 80 °C.

Introduction

Increasing attention has been paid to organic–inorganic hybrid molecules and polymers [1–5], which are advantageous for accurate molecular design and have excellent properties due to their organic synthesis and inorganic components, respectively. Polyhedral oligomeric silsesquioxane (POSS) is one of the representative building blocks used to construct such organic–inorganic hybrid materials [6–13]. This is because the chemical structure of a POSS can be easily modified by organic substituents and has a stable, transparent, and rigid inorganic core. These characteristics have led to the widespread application of a POSS in electronic devices, organic syntheses, biomaterials, etc. For further versatility of POSS-based materials, novel molecular designs are still desired. In particular, self-assembly of amphiphilic molecules is an effective bottom-up route to create highly functionalized and high-performance materials, and thus development of amphiphilic POSS derivatives is a promising strategy in this context.

The self-association behavior of hydrophobic POSS-containing amphiphilic polymers has been attracting attention [14–23]. Zhang et al. prepared hydrophilic poly(acrylic acid) (PAA) possessing a hydrophobic POSS moiety at one end (POSS-PAA) and at both ends (POSS-PAA-POSS) [20, 21]. In water, POSS-PAA and POSS-PAA-POSS form spherical and ellipsoidal aggregates, respectively. The aggregation numbers of these aggregates are much higher than those of conventional core-shell polymer micelles because the structures of the aggregates are not simple core-shell structures. The PAA chains are distributed into the hydrophobic POSS core. As another effect of hydrophobic POSS on the properties of hydrophilic polymers, the lower critical solution temperature (LCST) can be controlled to introduce the POSS group into a thermoresponsive polymer chain, such as poly(*N*-isopropylacrylamide) (PNIPAM). Zheng et al. introduced a hydrophobic POSS group at one end of a PNIPAM chain to reduce the solubility in water [22]. The LCST of the POSS-containing PNIPAM in water shifted to a lower temperature. Li et al. also reported the

Electronic supplementary material The online version of this article (https://doi.org/10.1038/s41428-017-0021-7) contains supplementary material, which is available to authorized users.

✉ Kensuke Naka
kenaka@kit.ac.jp

[1] Faculty of Molecular Chemistry and Engineering, Graduate School of Science and Technology, Kyoto Institute of Technology, Goshokaido-cho, Matsugasaki, Sakyo-ku, Kyoto 606-8585, Japan

[2] Department of Applied Chemistry, Graduate School of Engineering, University of Hyogo, 2167 Shosha, Himeji, Hyogo 671-2280, Japan

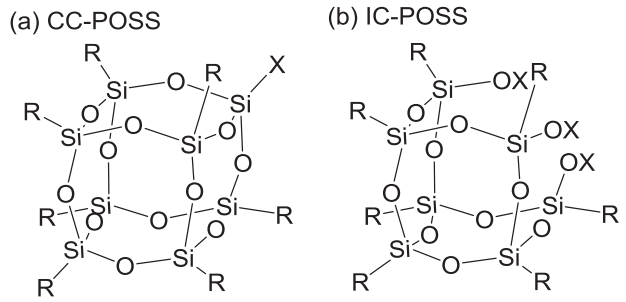

Fig. 1 Chemical structures of (**a**) CC-POSS and (**b**) IC-POSS

introduction of POSS at one end of a PNIPAM chain to adjust the LCST [23].

The aforementioned self-association behavior arises from the cubic structure of completely condensed POSS (CC-POSS) (Fig. 1a); the high crystallinity of CC-POSS promotes well-defined and robust assembly in some cases. On the other hand, the high crystallinity could often cause undesired aggregation to lower the dispersibility. To circumvent this drawback, we recently developed a novel material design based on an incompletely condensed POSS (IC-POSS), in which one corner of the cubic backbone is open (Fig. 1b) [24, 25]. We synthesized amphiphilic IC-POSSs possessing seven isobutyl groups at the corners and three poly(ethylene glycol) (PEG) chains at the opening moiety. Emulsions with the amphiphilic IC-POSSs are highly stable even 1 month after their preparation, while a CC-POSS analog cannot stabilize emulsions [24]. We also elucidated that the amphiphilic IC-POSSs form spherical micelles in water, but the CC-POSSs form vesicles under the same conditions; the different assembly behavior is caused by the difference in the crystallinity of the POSS-core structure [25]. These fundamental results motivated us to investigate amphiphilic IC-POSSs with substituents other than isobutyl groups. In this work, we synthesized cyclopentyl-trifluoropropyl, phenyl-trifluoropropyl, and (3,3,3-trifluoropropyl)-substituted amphiphilic IC-POSSs with two kinds of PEG chains ($M_n \simeq$ 600 and 2000), which formed micelle structures in water. The micelle structures were composed of a hydrophobic IC-POSS core and hydrophilic PEG shells. The micelles formed from the amphiphilic IC-POSS derivatives with the shorter PEG chains ($M_n \simeq 600$) in water exhibited the LCST behavior. On the other hand, the micelles with the longer PEGs ($M_n \simeq 2000$) did not exhibit the LCST behavior in water.

Experimental procedures

Materials

Tetrahydrofuran (THF), chloroform ($CHCl_3$), toluene, *n*-hexane, triethylamine (NEt_3), sodium hydroxide (NaOH), and magnesium sulfate anhydrous ($MgSO_4$) were purchased from Nacalai Tesque (Kyoto, Japan). Distilled water was purchased from Wako Pure Chemical Industry (Osaka, Japan). Trichlorosilane and chlorodimethylsilane were purchased from Tokyo Chemical Industry (Tokyo, Japan). A xylene solution (0.1 M) of platinum(0)-1,3-divinyl-1,1,3,3-tetramethyldisiloxane (Pt(dvs)) and PEG monomethyl ethers ($M_n = 550$ and 2000) were purchased from Sigma-Aldrich (Hattiesburg, Mississippi, US). Heptaisobutyl trisilanol POSS (**1a**) [26] and heptaphenyl trisilanol POSS (**1c**) [27] were purchased from Hybrid Plastics Inc. (Hattiesburg, Mississippi, US). Heptacyclopentyl trisilanol POSS (**1b**) [28] and hepta(3,3,3-trifluoropropyl) sodium trisilate POSS (**1d**) [29] were synthesized by following protocols in the literature. Amphiphilic IC-POSS derivatives **3a** and **4a** [24], H-substituted CC-POSS derivative **5a**, and monoallyl-substituted PEGs A-PEG600 and A-PEG2000 were prepared as described in our previous paper [24].

Instruments

^{1}H (400 MHz), ^{13}C (100 MHz), and ^{29}Si (80 MHz) nuclear magnetic resonance (NMR) spectra were recorded on a Bruker DPX-400 spectrometer (Bruker BioSpin GmbH, Rheinstetten, Germany) in $CDCl_3$ using Me_4Si as an internal standard. The following abbreviations are used: s, singlet; t, triplet; sep, septet; and m, multiplet. Preparative high-performance liquid chromatography (HPLC) for purification was performed on an LC-6AD instrument (Shimadzu) with a tandem column system consisting of two columns selected from Shodex KF-2001, KF-2002, and KF-2003 (Showa Denko, Tokyo, Japan); chloroform was used as the eluent. Dynamic light scattering (DLS) measurements were performed using a Malvern Zetasizer Nano ZS instrument (Malvern, Worcestershire, UK) equipped with a He-Ne laser (4.0 mW at 632.8 nm) at 25 °C. The obtained DLS data were analyzed to obtain the number-average hydrodynamic radius (R_h) distributions and polydispersity index (PDI) with Malvern Zetasizer software 7.11. The R_h value was calculated by the Stokes–Einstein equation, $R_h = k_B T/(6\pi\eta D)$, where k_B is the Boltzmann constant, T is the absolute temperature, η is the solvent viscosity, and D is the diffusion coefficient. The sample solutions were filtered through a 0.2 μm membrane filter. Percent transmittance ($\%T$) was measured using a Jasco V-630 BIO spectrophotometer equipped with a Jasco ETC-717 temperature controller (Tokyo, Japan). $\%T$ was monitored at 700 nm using a quartz cell with a 10 mm path length. Transmission electron microscopy (TEM) was performed using a Jeol JEM-2100 microscope (Jeol, Tokyo, Japan) at an accelerating voltage of 200 kV. One drop of the aqueous sample solution was placed on a copper grid coated with hydrated Formvar. The excess solution was blotted with filter paper. Then, one drop of an aqueous solution of sodium

phosphotungstate was placed on the grid for staining. The sample was dried under vacuum overnight.

Synthetic procedure and characterization data

Tris(dimethylsilyloxy)heptacyclopentyl IC-POSS (2b)

A THF solution (7 mL) of **1b** (0.51 g, 0.58 mmol) and NEt_3 (0.80 mL, 5.7 mmol) was cooled to 0 °C under a N_2 atmosphere, and chlorodimethylsilane (0.28 mL, 2.6 mmol) was added slowly. After stirring at 0 °C for 1 h and subsequently sitting at room temperature for 3 h, distilled water (2 mL) was added to quench the reaction. The volatiles were removed in vacuo, and the residue was extracted with *n*-hexane. The combined organic layers were dried over $MgSO_4$. After filtration and evaporation, the solvents were removed in vacuo to obtain **2b** (0.34 g, 0.44 mmol, 56%). ^{1}H-NMR ($CDCl_3$, 400 MHz) δ 4.75 (sep, $J = 2.8$ Hz, 3H), 1.81–1.69 (m, 14H), 1.64–1.56 (m, 14H), 1.54–1.46 (m, 28H), 0.94–0.89 (m, 7H), 0.24–0.23 (m, 18H) p.p.m. ^{13}C-NMR ($CDCl_3$, 100 MHz) δ 27.6, 27.3, 27.1, 27.0, 24.2, 23.5, 22.4, 0.7 ppm. ^{29}Si-NMR ($CDCl_3$, 80 MHz) δ −5.3, −66.0, −67.2, −67.9 p.p.m.

Tris(dimethylsilyloxy)heptaphenyl IC-POSS (2c)

A toluene solution (8 mL) of **1c** (0.44 g, 5.18 mmol) and NEt_3 (0.65 mL, 4.7 mmol) was cooled to 0 °C under a N_2 atmosphere, and a toluene solution (5 mL) of chlorodimethylsilane (0.25 mL, 2.25 mmol) was added slowly. After stirring at 0 °C for 1 h and subsequently sitting at room temperature for 3 h, distilled water (5 mL) was added to quench the reaction. The organic layer was separated and dried over $MgSO_4$. After filtration and evaporation, the solvents were removed in vacuo to obtain **2c** (0.46 g, 0.44 mmol, 87%). ^{1}H-NMR ($CDCl_3$, 400 MHz) δ 7.66–7.63 (m, 2H), 7.53–7.49 (m, 7H), 7.41–7.32 (m, 14H), 7.23–7.17 (m, 12H), 4.99 (sep, $J = 2.9$ Hz, 3H), 0.41–0.40 (m, 18H) p.p.m. ^{13}C-NMR ($CDCl_3$, 100 MHz) δ 134.1, 134.0, 132.5, 131.0, 130.7, 130.6, 130.3, 130.2, 128.0, 127.7, 127.6, 0.8 p.p.m. ^{29}Si-NMR ($CDCl_3$, 80 MHz) δ −2.7, −77.1, −77.5. −78.1 p.p.m.

Tris(dimethylsilyloxy)hepta(3,3,3-trifluoropropyl) IC-POSS (2d)

To a 1,2-dichloroethene solution (9 mL) of **1d** (0.61 g, 0.54 mmol) was slowly added a 1,2-dichloroethene solution (3.5 mL) of chlorodimethylsilane (0.90 mL, 8.1 mmol) at room temperature under a N_2 atmosphere. After stirring at 50 °C for 5 h, distilled water (9 mL) was added to quench the reaction. The organic layer was washed with distilled water and dried over $MgSO_4$. After filtration and evaporation, the solvents were removed in vacuo to obtain **2d** (0.48 g, 0.38 mmol, 71%). ^{1}H-NMR ($CDCl_3$, 400 MHz) δ 4.75 (sep, $J = 2.9$ Hz, 3H), 2.10–2.04 (m, 14H), 0.93–0.81 (m, 14H), 0.25–0.24 (m, 18H) p.p.m. ^{13}C-NMR ($CDCl_3$, 100 MHz) δ 131.1, 128.3, 125.6, 122.9, 28.4–27.2 (m), 5.6, 4.7, 3.9, 0.3 p.p.m. ^{19}F-NMR ($CDCl_3$, 377 MHz) δ −69.5 (t, $J = 10$ Hz), −69.9 (t, $J = 10$ Hz), −70.0 (t, $J = 10$ Hz) ppm. ^{29}Si-NMR ($CDCl_3$, 80 MHz) δ −2.3, −66.2, −68.5. −69.0 p.p.m.

TriPEG-substituted heptacyclopentyl IC-POSS (M_n of PEG = 600) (3b)

A THF solution (2 mL) of **2b** (185 mg, 0.177 mmol), A-PEG600 (730 mg, 1.23 mmol) and Pt(dvs) (0.1 M in xylene, 0.03 mL, 3.0×10^{-3} mmol) was refluxed for 6 h under a N_2 atmosphere. The solvents were removed in vacuo, and the residue was subjected to preparative HPLC to give **3b** (156 mg, 0.0593 mmol, 34%). ^{1}H-NMR ($CDCl_3$, 400 MHz) δ 3.65–3.57 and 3.38–3.33 (m, 145H), 1.74–1.64 (m, 14H), 1.60–1.49 (m, 20H), 1.49–1.32 (m, 28H), 0.92–0.76 (m, 7H), 0.51–0.45 (m, 6H), 0.07 (s, 18H) p.p.m. ^{13}C-NMR ($CDCl_3$, 100 MHz) δ 74.2, 71.9, 70.5, 69.9, 59.0, 27.6, 27.3, 27.0, 26.9, 24.5, 23.7, 23.3, 22.4, 14.0, 0.3 p.p.m. ^{29}Si-NMR ($CDCl_3$, 80 MHz) δ 8.9, −66.4, −67.7, −67.8 p.p.m.

TriPEG-substituted heptacyclopentyl IC-POSS (M_n of PEG = 2000) (4b)

The procedure was the same as that used for **3b**, except using A-PEG2000 instead of A-PEG600. The isolated yield was 26%. ^{1}H-NMR ($CDCl_3$, 400 MHz) δ 3.67–3.51 and 3.40–3.35 (m, 496H), 1.73–1.63 (m, 14H), 1.60–1.48 (m, 20H), 1.48–1.32 (m, 28H), 0.93–0.77 (m, 7H), 0.50–0.44 (m, 6H), 0.09 (s, 18H) p.p.m. ^{13}C-NMR ($CDCl_3$, 100 MHz) δ 74.1, 71.8, 70.5, 69.9, 58.9, 27.5, 27.1, 26.9, 26.8, 24.4, 23.6, 23.2, 22.3, 13.9, 0.3 p.p.m. ^{29}Si-NMR ($CDCl_3$, 80 MHz) δ 8.8, −66.5, −67.9, −68.0 p.p.m.

TriPEG-substituted heptaphenyl IC-POSS (M_n of PEG = 600) (3c)

A THF solution (2 mL) of **2c** (150 mg, 0.136 mmol), A-PEG600 (481 mg, 0.814 mmol) and Pt(dvs) (0.1 M in xylene, 0.01 mL, 1.0×10^{-3} mmol) was refluxed for 6 h under a N_2 atmosphere. The solvents were removed in vacuo, and the residue was subjected to preparative HPLC to give **3c** (103 mg, 0.0358 mmol, 26%). ^{1}H-NMR ($CDCl_3$, 400 MHz) δ 7.55–7.52 (m, 2H), 7.41–7.35 (m, 7H), 7.33–7.23 (m, 14H), 7.16–7.07 (m, 12H), 3.67–3.54 and 3.37–3.32 (m, 177H), 1.60–1.56 (m, 6H), 0.60–0.56 (m, 6H), 0.25 (s, 18H) p.p.m. ^{13}C-NMR ($CDCl_3$, 100 MHz) δ 133.9, 133.8, 132.7, 131.0, 130.6, 130.5, 130.2, 130.0, 127.9, 127.6, 127.5, 74.0, 71.9, 70.6, 69.9, 59.0, 23.2, 13.9, 0.3 p.p.m. ^{29}Si-NMR ($CDCl_3$, 80 MHz) δ 12.0, −77.4, −77.8, −78.1 p.p.m.

TriPEG-substituted heptaphenyl IC-POSS (M_n of PEG = 2000) (4c)

The procedure was the same as that for **3c**, except using A-PEG2000 instead of A-PEG600. The isolated yield was 36%. ^{1}H-NMR ($CDCl_3$, 400 MHz) δ 7.52–7.48 (m, 2H), 7.35–7.31 (m, 7H), 7.29–7.20 (m, 14H), 7.13–7.03 (m, 12H), 3.69–3.41 and 3.24–3.27 (m, 652H), 1.57–1.53 (m, 6H), 0.57–0.52 (m, 6H), 0.21 (s, 18H) p.p.m. ^{13}C-NMR ($CDCl_3$, 100 MHz) δ 133.8, 133.7, 132.6, 131.0, 130.6, 130.4, 130.1, 129.9, 127.8, 127.5, 127.4, 73.9, 71.9, 70.5, 69.8, 58.9, 23.1, 13.8, 0.2 ppm. ^{29}Si-NMR ($CDCl_3$, 80 MHz) δ 11.9, −77.5, −77.8, −78.1 p.p.m.

TriPEG-substituted hepta(3,3,3-trifluoropropyl) IC-POSS (M_n of PEG = 600) (3d)

A THF solution (1.5 mL) of **2d** (148 mg, 0.118 mmol), A-PEG600 (430 mg, 0.73 mmol) and Pt(dvs) (0.1 M in xylene, 0.015 mL, 1.5×10^{-3} mmol) was refluxed for 6 h under a N_2 atmosphere. The solvents were removed in vacuo, and the residue was subjected to preparative HPLC to give **3c** (95 mg, 0.032 mmol, 27%). ^{1}H-NMR ($CDCl_3$, 400 MHz) δ 3.67–3.52 and 3.42–3.36 (m, 132H), 2.09–2.01 (m, 14H), 1.55–1.53 (m, 6H), 0.84–0.75 (m, 14H), 0.54–0.51 (m, 6H), 0.03 (s, 18H) p.p.m. ^{13}C-NMR ($CDCl_3$, 100 MHz) δ 131.1, 128.3, 125.5, 122.8, 73.8, 71.9, 70.6, 70.1, 59.0, 28.2, 27.9, 27.6, 23.2, 13.8, 6.0, 4.8, 3.9, 0.1 p.p.m. ^{19}F-NMR ($CDCl_3$, 377 MHz) δ −69.4 (t, $J = 10$ Hz), −69.8 (t, $J = 10$ Hz), −69.9 (t, $J = 10$ Hz) p.p.m. ^{29}Si-NMR ($CDCl_3$, 80 MHz) δ 12.7, −66.3, −68.3, −69.6 p.p.m.

TriPEG-substituted hepta(3,3,3-trifluoropropyl) IC-POSS (M_n of PEG = 2000) (4d)

The procedure was the same as that for **3d**, except using A-PEG2000 instead of A-PEG600. The isolated yield was 17%. ^{1}H-NMR ($CDCl_3$, 400 MHz) δ 3.73–3.43 and 3.39–3.35 (m, 590H), 2.14–1.97 (m, 14H), 1.60–1.51 (m, 6H), 0.92–0.74 (m, 14H), 0.56–0.51 (m, 6H), 0.11 (s, 18H) p.p.m. ^{13}C-NMR ($CDCl_3$, 100 MHz) δ 131.0, 128.2, 125.5, 122.8, 73.7, 71.9, 70.5, 70.0, 58.9, 28.1, 27.8, 27.5, 23.2, 13.8, 5.9, 4.8, 3.9, 0.0 p.p.m. ^{19}F-NMR ($CDCl_3$, 377 MHz) δ -69.3 (t, $J = 10$ Hz), −69.7 (t, $J = 10$ Hz), −69.9 (t, $J = 10$ Hz) p.p.m. ^{29}Si-NMR ($CDCl_3$, 80 MHz) δ 12.6, −66.3, −68.3, −69.6 p.p.m.

Heptacyclopentyl CC-POSS (5b)

A THF solution (7 mL) of **1b** (510 mg, 0.58 mmol) and NEt_3 (0.90 mL, 6.5 mmol) was cooled to 0 °C under a N_2 atmosphere, and a THF solution (5 mL) of trichlorosilane (0.10 mL, 0.99 mmol) was added slowly. After stirring at 0 °C for 1 h and subsequently sitting at room temperature for 3 h, the volatiles were removed in vacuo. The residue was dissolved in hexane and washed with distilled water. The organic layer was separated and dried over $MgSO_4$. After filtration and evaporation, the solvents were removed in vacuo to obtain **5b** (70 mg, 0.075 mmol, 13%). ^{1}H-NMR ($CDCl_3$, 400 MHz) δ 4.12 (s, 1H), 1.78–1.70 (m, 14H), 1.62–1.54 (m, 14H), 1.54–1.42 (m, 28H), 1.05–0.92 (m, 7H) p.p.m. ^{13}C-NMR ($CDCl_3$, 100 MHz) δ 27.3, 27.2, 27.0, 26.9, 22.2, 22.1 p.p.m. ^{29}Si-NMR ($CDCl_3$, 80 MHz) δ −66.4, −66.5, −84.0 p.p.m.

Heptaphenyl CC-POSS (5c)

A toluene solution (8 mL) of **1c** (520 mg, 0.56 mmol) and NEt_3 (0.25 mL, 1.8 mmol) was cooled to 0 °C under a N_2 atmosphere, and a toluene solution (4 mL) of trichlorosilane (0.20 mL, 2.0 mmol) was added slowly. After stirring at 0 °C for 1.5 h, the volatiles were removed in vacuo. The residue was dissolved in $CHCl_3$ and washed with distilled water. The organic layer was separated and dried over $MgSO_4$. After filtration, the solution was poured into methanol to obtain precipitates of **5c** (150 mg, 0.16 mmol, 28%). ^{1}H-NMR ($CDCl_3$, 400 MHz) δ 7.79–7.71 (m, 7H), 7.48–7.40 (m, 14H), 7.40-7.31 (m, 28H), 4.51 (s, 1H) p.p.m. ^{13}C-NMR ($CDCl_3$, 100 MHz) δ 134.2, 134.1, 130.9, 130.8, 130.0, 129.9, 127.9, 127.8 ppm. ^{29}Si-NMR ($CDCl_3$, 80 MHz) δ −78.3, −78.6, −83.0 p.p.m.

Preparation of aqueous solutions

Aqueous polymer solutions were prepared with a polymer concentration (C_p) = 10 g/L. The aqueous solutions were stirred overnight at room temperature prior to measurements. TEM samples were diluted with pure water to attain $C_p = 1.0$ g/L.

Results and discussion

Synthesis of amphiphilic IC-POSSs

To compare alkyl, cycloalkyl, aryl, and fluoroalkyl groups, IC-POSS trisilanols with alkyl isobutyl [26], cyclopentyl [28], phenyl [27], and trifluoropropyl [29] groups (**1a–d**, respectively) were prepared (**1d** was obtained as the sodium salt) because the synthetic protocols for these IC-POSS derivatives are well established. In addition, the amount of the hydrophilic component is crucial, and thus, two kinds of PEGs possessing an allyl group at one terminal were synthesized and denoted A-PEG600 and A-PEG2000 according to their molecular weight ($M_n \simeq 600$ and 2000, respectively). Amphiphilic POSS derivatives were

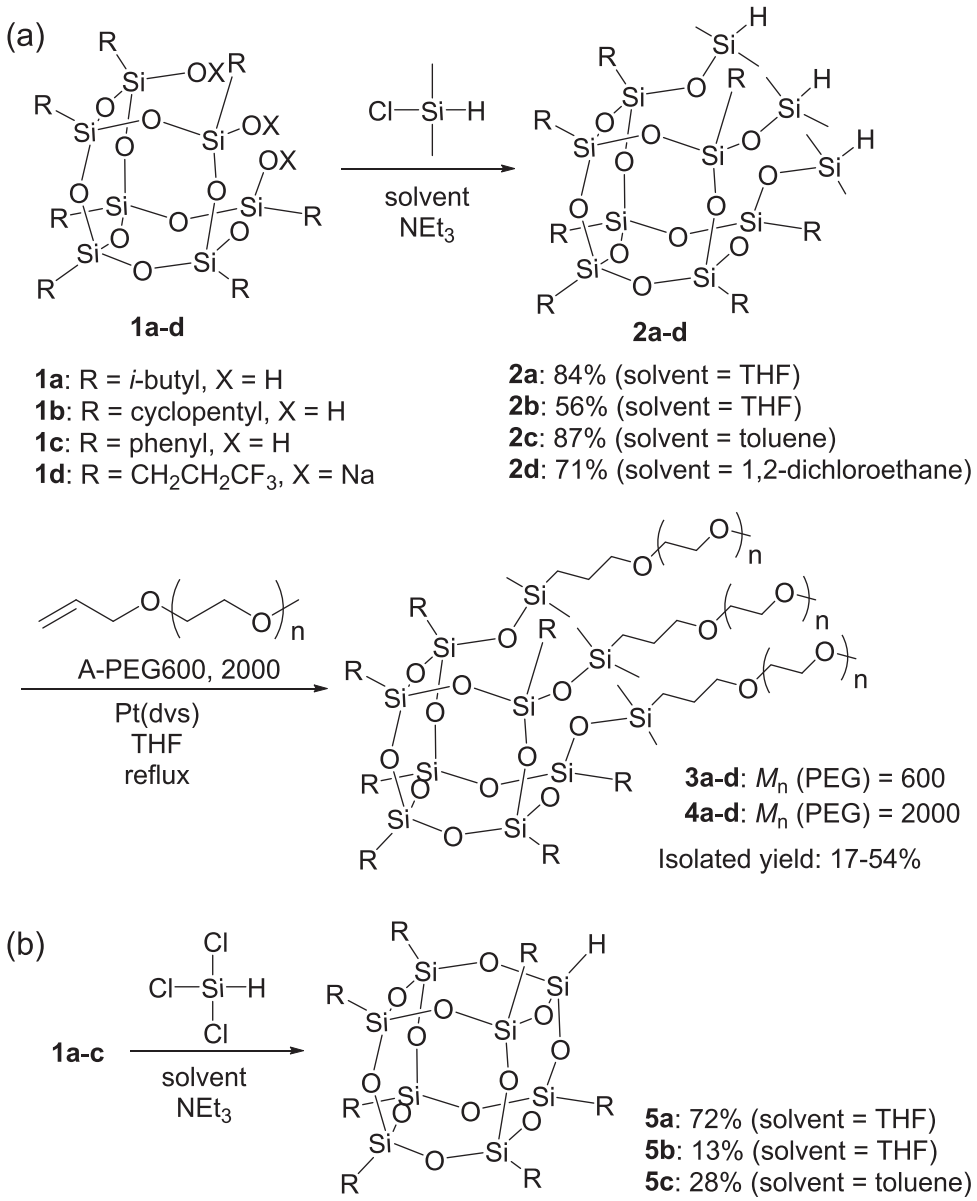

Scheme 1 Syntheses of (**a**) amphiphilic IC-POSSs and (**b**) H-substituted CC-POSSs

synthesized by utilizing these compounds as shown in Scheme 1a. Condensation of the three silanol groups of **1a–d** with chlorodimethylsilane gave **2a–d**, according to a previous study [24]. The platinum-catalyzed hydrosilylation of **2a–d** with A-PEG600 and A-PEG2000 produced **3a–d** (from A-PEG600) and **4a–d** (from A-PEG2000). Purification of the amphiphilic IC-POSSs was carried out by preparative HPLC to remove di-substituted and mono-substituted by-products and unreacted PEGs. The chemical structures of **3a–d** and **4a–d** were determined from their ^{1}H-NMR, ^{13}C-NMR, ^{19}F-NMR, and ^{29}Si-NMR spectra. In addition to the IC-POSS **2a–d**, the CC-POSS analogs **5a–c** were prepared (Scheme 1b) to compare the thermal properties of IC-POSS and CC-POSS (*vide infra*). Although we tried to synthesize hepta(3,3,3-trifluoropropyl)POSS, small amounts of undetermined impurities were contained in the product, and thermal analyses were unable to be performed.

Thermal properties of amphiphilic POSSs

Thermogravimetric analysis (TGA) and differential scanning calorimetry (DSC) of **2a–d** and **5a–c** were carried out (Fig. 2) to compare the thermal stability and crystallinity of the IC-POSSs and CC-POSSs. The degradation temperatures for 5 and 10% weight loss (T_{d5} and T_{d10}, respectively) and the melting points (T_m) are summarized in Table 1. The degradation temperatures of **2a** ($T_{d5} = 219$ °C, $T_{d10} = 234$ °C) [24] and **2b** ($T_{d5} = 299$ °C, $T_{d10} = 316$ °C) were not significantly different from those of **5a** ($T_{d5} = 228$ °C, $T_{d10} = 242$ °C) and **5b** ($T_{d5} = 308$ °C, $T_{d10} = 325$ °C),

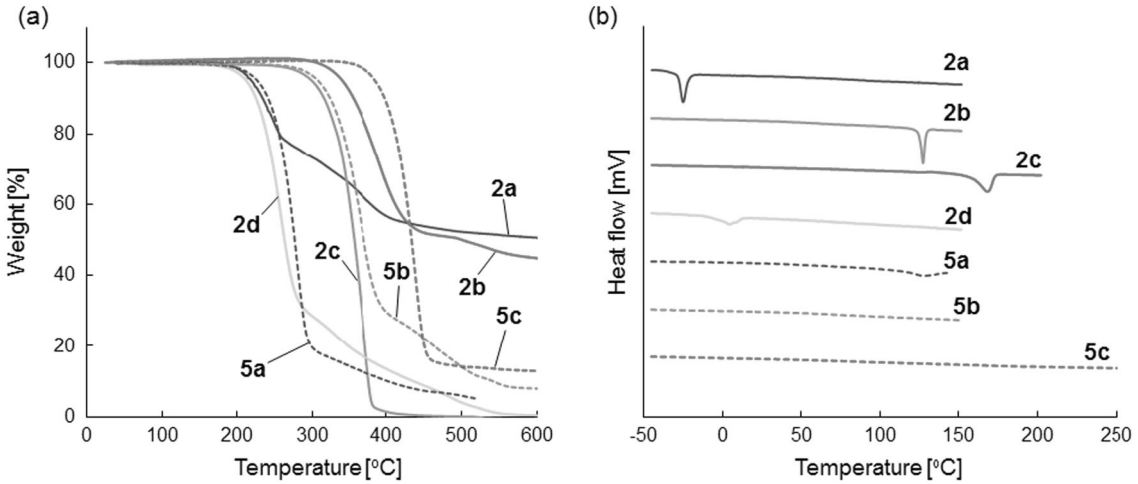

Fig. 2 **a** TGA thermograms and **b** DSC curves of IC-POSS (solid lines) and CC-POSSs (dashed lines) (Color figure online)

Table 1 Thermal properties

R[a]	Compound	T_{d5}/T_{d10}[b] [°C]	T_m[c] [°C]
i-Bu	**2a**[d]	219 / 234	−25
	5a[d]	228 / 242	138
Cy	**2b**	299 / 316	127
	5b	308 / 325	n.d.[e]
Ph	**2c**	340 / 355	170
	5c	385 / 398	n.d.[e]
TFP	**2d**	213 / 226	4

[a] *i*-Bu isobuty, Cy cyclopentyl, Ph phenyl, TFP 3,3,3-trifluoropropyl

[b] Measured by TGA

[c] Measured by DSC

[d] Reference [24]

[e] Not detected

respectively. The alkyl groups, i.e., isobutyl, cyclopentyl, and trifluoropropyl groups, decomposed in the early stage of the TGA. The thermal stability of these organic substituents was provided by the IC-POSS and CC-POSS cores in the same fashion. On the other hand, IC-POSS **2c** showed weight loss at a lower temperature ($T_{d5} = 340$ °C, $T_{d10} = 355$ °C) than CC-POSS **5c** ($T_{d5} = 385$ °C, $T_{d10} = 398$ °C). In the high-temperature region (>300 °C), the thermal stability of the rigid CC-POSS was distinguished from that of the flexible IC-POSS; the thermal durability of the phenyl groups was responsible for the difference. Nonetheless, **2c** also possessed high thermal stability, and it has been demonstrated that IC-POSS offers high stability to organic substituents. Trifluoropropyl-substituted IC-POSS **2d** was the most thermally unstable and had a low melting temperature probably because trifluoropropyl-substituted POSS has weaker intermolecular interactions than POSS with other substituents, as we previously reported [30].

As we previously reported, the T_m of **2a** (−25 °C) was drastically lower than that of **5a** (138 °C) [24]. CC-POSSs **5b** and **5c** did not melt probably because their melting points are higher than their decomposition temperatures. In contrast, IC-POSSs **2b** and **2c** showed melting points at 127 and 170 °C, respectively. These results mean that the crystallinity of POSS can be effectively lowered by adopting an open cage structure. It has been confirmed that IC-POSS is an excellent molecular design that drastically lowers the crystallinity with no or slight deterioration of the thermal stability.

Self-assembly structure in water

The hydrodynamic radius (R_h) distributions for **3a–d** and **4a–d** in pure water were measured by dynamic light scattering (DLS) (Fig. 3). The R_h and polydispersity index (PDI) values are summarized in Table 2. All the R_h distributions were unimodal. The R_h values for **3a–d** and **4a–d** were 4–8 nm. The PDI values for **3a–d** and **4a** were relatively narrow (0.13–0.20). These amphiphilic IC-POSSs may form core-shell spherical micelles due to intermolecular self-association in water. The hydrophobic IC-POSSs containing isobutyl, cyclopentyl, phenyl, and 3,3,3-trifluoropropyl substituents formed the core, and the hydrophilic PEG formed the shells. As a representative example, the ^{1}H-NMR spectrum of **3b** was measured in D_2O, and relatively sharp peaks for the PEG chains were observed with broad signals due to the cyclopentyl groups. This means that the hydrophobic cyclopentyl groups

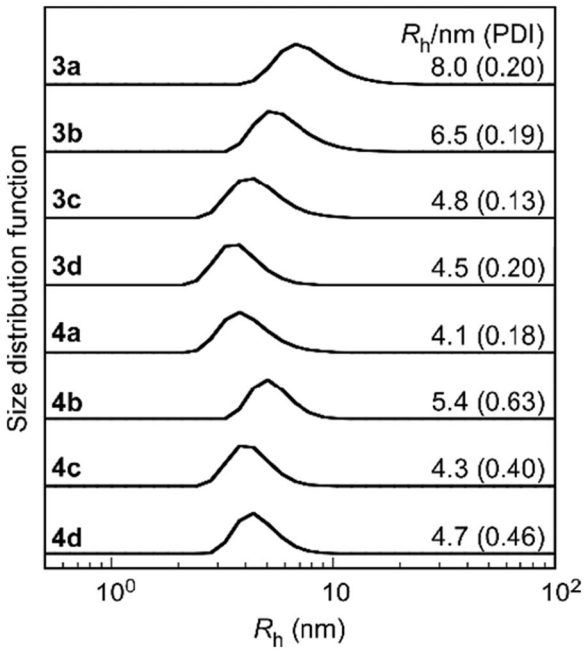

Fig. 3 Hydrodynamic radius (R_h) number distributions with the polydispersity index (PDI) for IC-POSS-PEG600 and IC-POSS-PEG2000 substituted with isobutyl (**3a**, **4a**), cyclopentyl (**3b**, **4b**), phenyl (**3c**, **4c**), and 3,3,3-trifluoropropyl (**3d**, **4d**) in water at 25 °C at concentrations of 10 g/L

Table 2 Hydrodynamic radius (R_h), polydispersity index (PDI), radius (R_{TEM}) estimated from transmission electron microscopy (TEM) images, and lower critical solution temperature (LCST)

Compound	R_h (nm)	PDI	R_{TEM} (nm)	LCST[a] (°C)
3a	8.0	0.20	10.4	39 (37)
3b	6.5	0.19	12.0	45 (44)
3c	4.8	0.13	8.6	39 (41)
3d	4.5	0.43	14.3	48 (47)
4a	4.1	0.20	12.1	–
4b	5.4	0.63	8.1	–
4c	4.3	0.40	13.8	–
4d	4.7	0.46	10.1	–

[a] Temperature was estimated while heating, and the temperature in parentheses was estimated while cooling

densely pack together to form the core-shell structures (Figure S37). The PDI values for **4b–d** were broad (0.40–0.63). The large PDI suggests that the micelles may contain a small amount of intermicellar aggregates. The DLS data were analyzed based on the R_h number distributions. The small amounts of intermicellar aggregates with larger sizes were negligible in the R_h number distributions. The R_h values of IC-POSSs with PEG2000 (**4a**, **4b**, and **4c**) were smaller than those of IC-POSSs with PEG600 (**3a**, **3b**, and **3c**). The R_h value of **4d** was larger than that of **3d** presumably because the PDI of **4d** was extremely large. These observations suggest that IC-POSSs with longer PEG chains tend to form smaller aggregates.

TEM observations were performed for **3a–d** and **4a–d** (Fig. 4). Magnified TEM images are indicated in Figure S38. Almost spherical objects can be observed for all samples. To determine the radius (R_{TEM}) values from TEM, more than 50 particles were selected randomly. The average radii were calculated and used as the R_{TEM} values. The R_{TEM} values were always larger than R_h (Table 2) possibly because of the difficulty of observing small molecules by TEM. To observe small objects, the TEM electron beam must be focused. Therefore, organic-inorganic hybrid samples are easily decomposed. Furthermore, the boundaries of particles in the TEM observations were not clear because it was difficult to stain the TEM samples. Therefore, the R_{TEM} values may contain error.

Lower critical solution temperature (LCST) behavior

%T values for the aqueous solutions of **3a–d** were measured as a function of temperature to determine the lower critical solution temperature (LCST) with heating (Fig. 5). *%T* was zero for the aqueous solutions of **3a–d** above the LCST, and precipitates formed over time, making the solutions heterogeneous. In this study, *%T* vs. temperature plots were determined for the solutions with stirring. The LCST was defined as the temperature where *%T* started to decrease sharply with heating. The *%T* vs. temperature plots for **3a–d** indicated slight hysteresis with heating and cooling (Figure S39). With cooling, the LCST was defined as the temperature where *%T* became constant. The LCSTs for **3a–d** were observed from 39–48 °C. The obtained LCSTs are summarized in Table 2. The LCST behavior was not able to be observed in the aqueous solutions of **4a–d** (Figure S40). Although the ether groups in the PEG chains can form hydrogen bonds with water molecules to hydrate the PEG chains, molecular motions increase hydrogen bond breakage, leading to dehydration with increasing temperature [31, 32]. In general, PEG has a phase transition temperature above 100 °C in water. Hydrophobic substituents on PEG chains should decrease the phase transition temperature in water because the substituents promote dehydration. When hydrophobic IC-POSS was introduced to PEG600 chains (**3a–d**), the LCST was observed due to the promotion of dehydration by the PEG chains. On the other hand, for PEG2000, PEG with hydrophobic IC-POSS (**4a–d**) did not show the LCST because the whole PEG2000 chains could not be dehydrated with increasing temperature.

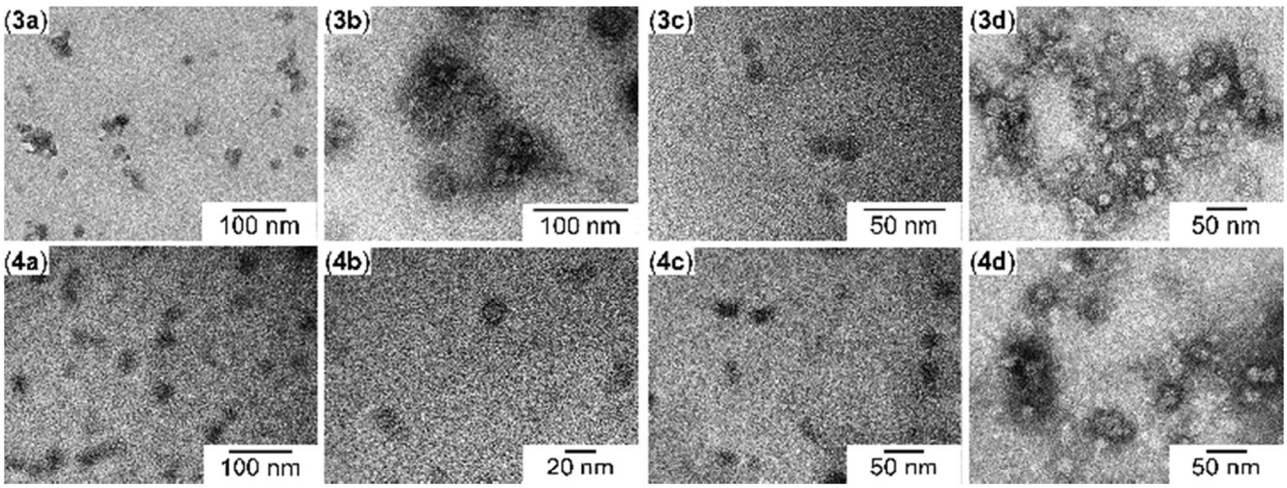

Fig. 4 TEM images of IC-POSS-PEG600 (**3**) and IC-POSS-PEG2000 (**4**) substituted with isobutyl (**3a**, **4a**), cyclopentyl (**3b**, **4b**), phenyl (**3c**, **4c**), and 3,3,3-trifluoropropyl (**3d**, **4d**)

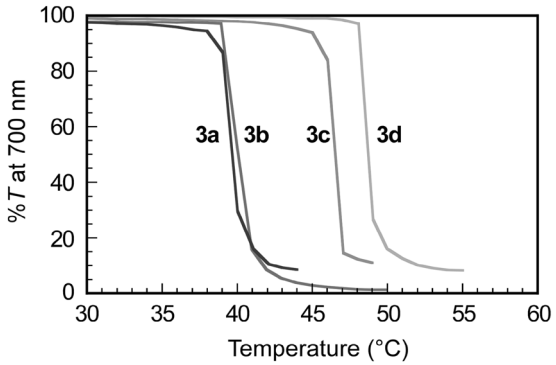

Fig. 5 Percent transmittance (%*T*) of aqueous solutions of **3a** (blue), **3b** (red), **3c** (green), and **3d** (yellow) as a function of temperature during heating (Color figure online)

Conclusions

In summary, we synthesized new amphiphilic IC-POSS derivatives possessing various kinds of substituents and two kinds of PEGs with different chain lengths. The IC-POSS cores had lower crystallinity than the CC-POSS analogs, and the thermal stability of the IC-POSS cores was sufficiently high. DLS and TEM measurements revealed that the amphiphilic IC-POSSs formed micelles in water with unimodal size distributions. The structures of the substituents on the seven Si atoms and the chain length of PEGs affected the association behavior of the amphiphilic IC-POSSs—the LCST significantly changed depending on the PEG chain length. This is the first study on the self-association of amphiphilic IC-POSSs with various substituents, which are promising building blocks for organic-inorganic hybrid architectures. We are now investigating the utilization of the high dispersibility of IC-POSSs in various matrices toward the preparation of unprecedented materials.

Acknowledgements HI acknowledges a Grant-in-Aid for Young Scientists (B) (JSPS KAKENHI Grant Number JP17H05369).

Compliance with ethical standards

Conflict of interest The author declares that they have no conflict of interest.

References

1. Nishimura T. Macromolecular templates for the development of organic/inorganic hybrid materials. Polym J. 2015;47:235–43.
2. Kaushik A, Kumar R, Arya SK, Nair M, Malhotra BD, Bhansali S. Organic–inorganic hybrid nanocomposite-based gas sensors for environmental monitoring. Chem Rev. 2015;115:4571–606.
3. Sun Z, Cui G, Li H, Liu Y, Tian Y, Yan S. Multifunctional optical sensing probes based on organic–inorganic hybrid composites. J Mater Chem B. 2016;4:5194–216.
4. Shimizu T, Kanamori K, Nakanishi K. Silicone-based organic–inorganic hybrid aerogels and xerogels. Chem Eur J. 2017;23:5176–87.
5. Gon M, Tanaka K, Chujo Y. Creative synthesis of organic–inorganic molecular hybrid materials. Bull Chem Soc Jpn. 2017;90:463–74.
6. Laine RM, Zhang C, Sellinger A, Viculis L. Polyfunctional cubic silsesquioxanes as building blocks for organic/inorganic hybrids. Appl Organo Chem. 1998;12:715–23.
7. Laine RM. Nanobuilding blocks based on the $[OSiO_{1.5}]_x$ (x = 6, 8, 10) octasilsesquioxanes. J Mater Chem. 2005;15:3725–44.
8. Cordes DB, Lickiss PD, Rataboul F. Recent developments in the chemistry of cubic polyhedral oligosilsesquioxanes. Chem Rev. 2010;110:2081–173.
9. Tanaka K, Chujo Y. Chemicals-inspired biomaterials: developing biomaterials inspired by material science based on POSS. Bull Chem Soc Jpn. 2013;86:1231–9.
10. Chujo Y, Tanaka K. New polymeric materials based on element-blocks. Bull Chem Soc Jpn. 2015;88:633–43.

11. Ye Q, Zhou H, Xu J. Cubic polyhedral oligomeric silsesquioxane based functional materials: synthesis, assembly, and applications. Chem Asian J. 2016;11:1322–37.
12. Naka K, Irie Y. Synthesis of single component element-block materials based on siloxane-based cage frameworks. Polym Int. 2017;66:187–94.
13. Li Z, Kong J, Wang F, He C. Polyhedral oligomeric silsesquioxanes (POSSs): an important building block for organic optoelectronic materials. J Mater Chem C. 2017;5: 5283–98.
14. Takeda M, Kuroiwa K, Mitsuishi M, Matsui J. Self assembly of amphiphilic POSS anchoring a short organic tail with uniform structure. Chem Lett. 2015;44:1560–2.
15. Li L, Lu B, Fan Q, Wu J, Wei L, Hou J, Guo X, Liu Z. Synthesis and self-assembly behavior of pH-responsive star-shaped POSS-(PCL-P(DMAEMA-*co*-PEGMA))$_{16}$ inorganic/organic hybrid block copolymer for the controlled intracellular delivery of doxorubicin. RSC Adv. 2016;6:61630–40.
16. Peng W, Xu S, Li L, Zhang C, Zheng S. Organic–inorganic nanocomposites via self-assembly of an amphiphilic triblock copolymer bearing a Poly(butadiene-*g*-POSS) subchain in epoxy thermosets: morphologies, surface hydrophobicity, and dielectric properties. J Phys Chem B. 2016;120:12003–14.
17. Zhang Z, Xue Y, Zhang P, Müller AHE, Zhang W. Hollow polymeric capsules from poss-based block copolymer for photodynamic therapy. Macromolecules. 2016;49:8440–8.
18. Shao Y, Yin G-Y, Ren X, Zhang X, Wang J, Guo K, Li X, Wesdemiotis C, Zhang W-B, Yang S, Zhu M, Sun B. Engineering π–π interactions for enhanced photoluminescent properties: unique discrete dimeric packing of perylene diimides. RSC Adv. 2017;7:6530–7.
19. Li C, Li X, Tao C, Ren L, Zhao Y, Bai S, Yuan X. Amphiphilic antifogging/anti-icing coatings containing POSS-PDMAEMA-*b*-PSBMA. ACS Appl Mater Interfaces. 2017;9:22959–69.
20. Zhang W, Fang B, Walther A, Muller AHE. Synthesis via RAFT polymerization of tadpole-shaped organic/inorganic hybrid Poly (acrylic acid) containing polyhedral oligomeric silsesquioxane (POSS) and their self-assembly in water. Macromolecules. 2009;42:2563–9.
21. Zhang W, Yuan J, Weiss S, Ye X, Li C, Müller AHE. Telechelic hybrid Poly(acrylic acid)s containing polyhedral oligomeric silsesquioxane (POSS) and their self-assembly in water. Macromolecules. 2011;44:6891–8.
22. Zheng Y, Wang L, Zheng S. Synthesis and characterization of heptaphenyl polyhedral oligomeric silsesquioxane-capped poly(*N*-isopropylacrylamide)s. Eur Polym J. 2012;48:945–55.
23. Li M, Song X, Zhang T, Zeng L, Xing J. Aggregation induced emission controlled by a temperature-sensitive organic–inorganic hybrid polymer with a particular LCST. RSC Adv. 2016;6:86012–8.
24. Imoto H, Nakao Y, Nishizawa N, Fujii S, Nakamura Y, Naka K. Tripodal polyhedral oligomeric silsesquioxanes as a novel class of three-dimensional emulsifiers. Polym J. 2015;47:609–15.
25. Yusa S, Ohno S, Honda T, Imoto H, Nakao Y, Naka K, Nakamura Y, Fujii S. RSC Adv. 2016;6:73006–12.
26. Zhou J, Zhao Y, Yu K, Zhou X, Xie X. Synthesis, thermal stability and photoresponsive behaviors of azobenzene-tethered polyhedral oligomeric silsesquioxanes. New J Chem. 2011;35:2781–92.
27. Hu J, Li L, Zhang S, Gong L, Gong S. Novel phenyl-POSS/polyurethane aqueous dispersions and their hybrid coatings. J Appl Polym Sci. 2013;130:1611–20.
28. Fehr FJ, Budzichowski TA, Blanski RL, Weller KJ, Ziller JW. Facile syntheses of new incompletely condensed polyhedral oligosilsesquioxanes: [(*c*-C_5H_9)$_7$$Si_7O_9(OH)_3$], [(*c*-$C_7H_{13}$)$_7$$Si_7O_9(OH)_3$], and [(*c*-$C_7H_{13}$)$_6$$Si_6O_7(OH)_4$]. Organometallics. 1991;10:2526–8.
29. Koh K, Sugiyama S, Morinaga T, Ohno K, Tsujii Y, Fukuda T, Yamahiro M, Iijima T, Oikawa H, Watanabe K, Miyashita T. Precision synthesis of a fluorinated polyhedral oligomeric silsesquioxane-terminated polymer and surface characterization of its blend film with Poly(methyl methacrylate). Macromolecules. 2005;38:1264–70.
30. Araki H, Naka K. Syntheses and properties of star- and dumbbell-shaped POSS derivatives containing isobutyl groups. Polym J. 2012;44:340–6.
31. Bae YC, Lambert SM, Soane DS, Prausnitz JM. Cloud-point curves of polymer solutions from thermooptical measurements. Macromolecules. 1991;24:4403–7.
32. Ashbaugh HS, Paulaitis ME. Monomer hydrophobicity as a mechanism for the LCST behavior of Poly(ethylene oxide) in water. Ind Eng Chem Res. 2006;45:5531–7.